DISCOVER-EEG: an open, fully automated EEG pipeline for biomarker discovery in clinical neuroscience

Cristina Gil Ávila[1,2,3], Felix S. Bott[1,2], Laura Tiemann[1,2], Vanessa D. Hohn[1,2], Elisabeth S. May[1,2], Moritz M. Nickel[1,2], Paul Theo Zebhauser[1,2,4], Joachim Gross[5], Markus Ploner[1,2,4]

[1]Technical University of Munich, Germany; TUM School of Medicine, Department of Neurology

[2]Technical University of Munich, Germany; TUM School of Medicine, TUM-Neuroimaging Center

[3]Ludwig-Maximilians-Universität München, Munich, Germany; Graduate School of Systemic Neurosciences

[4]Technical University of Munich, Germany; TUM School of Medicine, Center for Interdisciplinary Pain Medicine

[5]University of Münster, Germany; Institute for Biomagnetism and Biosignalanalysis

Correspondence to:

Markus Ploner, Department of Neurology, Technical University of Munich,
Ismaninger Str. 22, 81675 Munich, Germany, markus.ploner@tum.de

ABSTRACT

Biomarker discovery in neurological and psychiatric disorders critically depends on reproducible and transparent methods applied to large-scale datasets. Electroencephalography (EEG) is a promising tool for identifying biomarkers. However, recording, preprocessing and analysis of EEG data is time-consuming and mostly subjective. Therefore, we developed DISCOVER-EEG, an open and fully automated pipeline that enables easy and fast preprocessing, analysis and visualization of resting state EEG data. Data in the standard EEG-BIDS structure are automatically preprocessed and physiologically meaningful features of brain function (including oscillatory power, connectivity and network characteristics) are extracted and visualized using two open-source and widely used Matlab toolboxes (EEGlab and FieldTrip). We exemplify the use of the pipeline for biomarker discovery in healthy ageing in the LEMON dataset, containing 212 healthy participants. We demonstrate its utility to speed up biomarker discovery in a clinical setting with a new dataset containing 74 patients with chronic pain. Thus, the DISCOVER-EEG pipeline facilitates the aggregation, reuse and analysis of large EEG datasets, promoting open and reproducible research on brain function.

INTRODUCTION

Biomarkers that relate brain function to cognitive and clinical phenotypes can help in the prediction, treatment, monitoring and diagnosis of neurological and psychiatric disorders[1,2]. The successful identification of biomarkers crucially depends on the application of reproducible and transparent methods[3] to large-scale datasets[4]. Furthermore, to translate biomarkers into clinical practice, they need to be generalizable, interpretable and easy to deploy in clinical settings.

Electroencephalography (EEG) is a promising tool for biomarker discovery, as it is non-invasive, safe, widely used in clinical and research contexts, portable and cost-efficient. Consequently, EEG biomarker candidates have been described in depression[5-7], post-traumatic stress disorder[7,8] and chronic pain[9]. Most of these biomarker candidates have been discovered in resting state data, during which spontaneous neural activity is captured. However, the acquisition of EEG data is often laborious and the preprocessing and analysis of EEG data involve manual steps that are time-consuming, subjective and dependent on expert knowledge. Thus, EEG datasets often have small sample sizes and low replicability[10], hindering their use for biomarker discovery.

In recent years, technological advances have expedited EEG data collection. For instance, mobile and dry-electrode headsets now allow for much faster data acquisition than traditional EEG setups with wet electrodes[11]. Moreover, progress has been achieved in automatizing and speeding up EEG preprocessing[12-15]. In addition, recent EEG-based connectivity and network measures have been shown to provide crucial information about brain function in neuropsychiatric disorders[16-18]. These advances can significantly further the development of EEG-based biomarkers of neuropsychiatric disorders. However, a complete and transparent workflow integrating all these elements to promote biomarker discovery in large cohorts of participants is still missing.

Here, we present DISCOVER-EEG, a comprehensive EEG pipeline for fast aggregation, preprocessing and analysis of resting state EEG data. So far, there is no single tool that automatically preprocesses EEG data and extracts physiologically meaningful EEG features (like oscillatory power, connectivity, network characteristics) for use in biomarker identification. Our pipeline accomplishes this goal in an easy-to-use manner building upon and combining well-established toolboxes for EEG preprocessing and analysis. It thereby facilitates the aggregation and analysis of large-scale datasets, as it is applicable to a wide range of EEG set-ups, including mobile and dry-electrode systems, and fosters sharing and reusability of the data by handling EEG-BIDS standardized data[19]. Additionally, it can be applied to healthy populations as well as populations with different neuropsychiatric disorders, extending its use to different research and clinical contexts.

We demonstrate the use of this pipeline in two openly-available resting state EEG datasets. In the first one, the LEMON dataset[20] including 212 young and old healthy participants, we show how reusing a dataset can inspire the discovery of biomarkers in healthy ageing. We specifically present an example analysis investigating differences in EEG features between old and young healthy populations. In the second one, we present a new dataset part of an ongoing project on biomarker discovery in chronic pain. To date, it includes 74 patients with chronic pain recorded with a mobile dry-electrode EEG system in a clinical setting. The application of the DISCOVER-EEG pipeline to this dataset demonstrates how to facilitate and speed up the acquisition and processing of large new datasets for the discovery of robust and reliable biomarkers.

METHODS

Design principles

Open-source and FAIR code

We developed an automated workflow for fast preprocessing, analysis and visualization of resting state EEG data (Figure 1) following open science and FAIR principles (Findability, Accessibility, Interoperability and Reusability)[21]. The code of the DISCOVER-EEG pipeline is published on GitHub and linked to an OSF project (https://osf.io/mru42/), which is thoroughly documented and uniquely referenced by a DOI (*Findability*). The code can be easily downloaded (*Accessibility*) and receive contributions (please refer to the section *Code availability*). To ensure its *Interoperability* and *Reusability*, the pipeline is based on two open-source Matlab toolboxes, EEGLab and FieldTrip[22], which are widely used, maintained and supported by the developers and the neuroimaging community (i.e. through forums and mailing lists). Basing the pipeline on validated and established software ensures its compatibility with future software updates. Moreover, it facilitates the interaction with experts in EEG analysis, who also gave advice and supported the pipeline during its development. The code of the current pipeline is intended to represent a basis that will integrate and benefit from feedback of the neuroimaging community.

Data reusability and large-scale data handling

As biomarker discovery needs large datasets, we designed the pipeline in view of data reusability and large-scale data handling. To this end, we followed the FAIR principles of scientific data management[23] and incorporated the EEG-BIDS standardized data structure[19] as a mandatory input of the pipeline. Most EEG setups and electrode configurations are compatible with the pipeline thanks to the EEGLab plugin *bids-matlab-tools.* Additionally, we tested that the pipeline is compatible with data recorded by mobile EEG devices with dry electrodes, which further facilitates the fast creation of large EEG datasets.

The pipeline was designed for resting state EEG data, during which spontaneous neural activity is recorded. Resting state data can be recorded easily in healthy and patient populations, in different study designs (e.g. cross-sectional, longitudinal) and in different types of neuropsychiatric disorders. Therefore, the use of resting state data facilitates the application to different settings and research questions. EEG recordings might also be accompanied by standardized patient reported outcomes, such as the PROMIS questionnaires[24], which can assess symptoms (e.g., pain, fatigue, anxiety, depression) across different neuropsychiatric disorders and thus, enable cross-disorder analyses. Together, these considerations contribute to the scalability and generalizability of the workflow.

Ease of use, transparency and interpretability

The pipeline was designed to be easy to use, in order to make it also accessible to those EEG users who are not proficient in coding. It consists of two main functions: *main_pipeline.m*, in which the preprocessing, feature extraction and visualization of the data are carried out, and *define_params.m*, in which parameters for preprocessing and feature extraction are defined. This latter file is the only one that needs to be adapted to the dataset and/or user-specific demands. When executing the pipeline, parameters are saved to a separate file to ensure reproducibility.

Additionally, the pipeline focuses on transparency and interpretability of results. For that reason, a PDF report is generated for each recording, in which the intermediate steps of the preprocessing (Figure 2) and the extracted EEG features (Figure 3) are visualized. These visualizations can serve as quality control checkpoints and help to detect shorter or corrupted files, misalignment of electrodes or missing data through fast visual inspection[25]. Along with their visualization, the preprocessed data and the extracted features of each recording are

saved to separate files that can be later used for statistical group analysis and/or biomarker discovery. These output files can be easily imported to other statistical packages or working environments, such as R or Python[26],e.g., for applying machine learning or deep learning models.

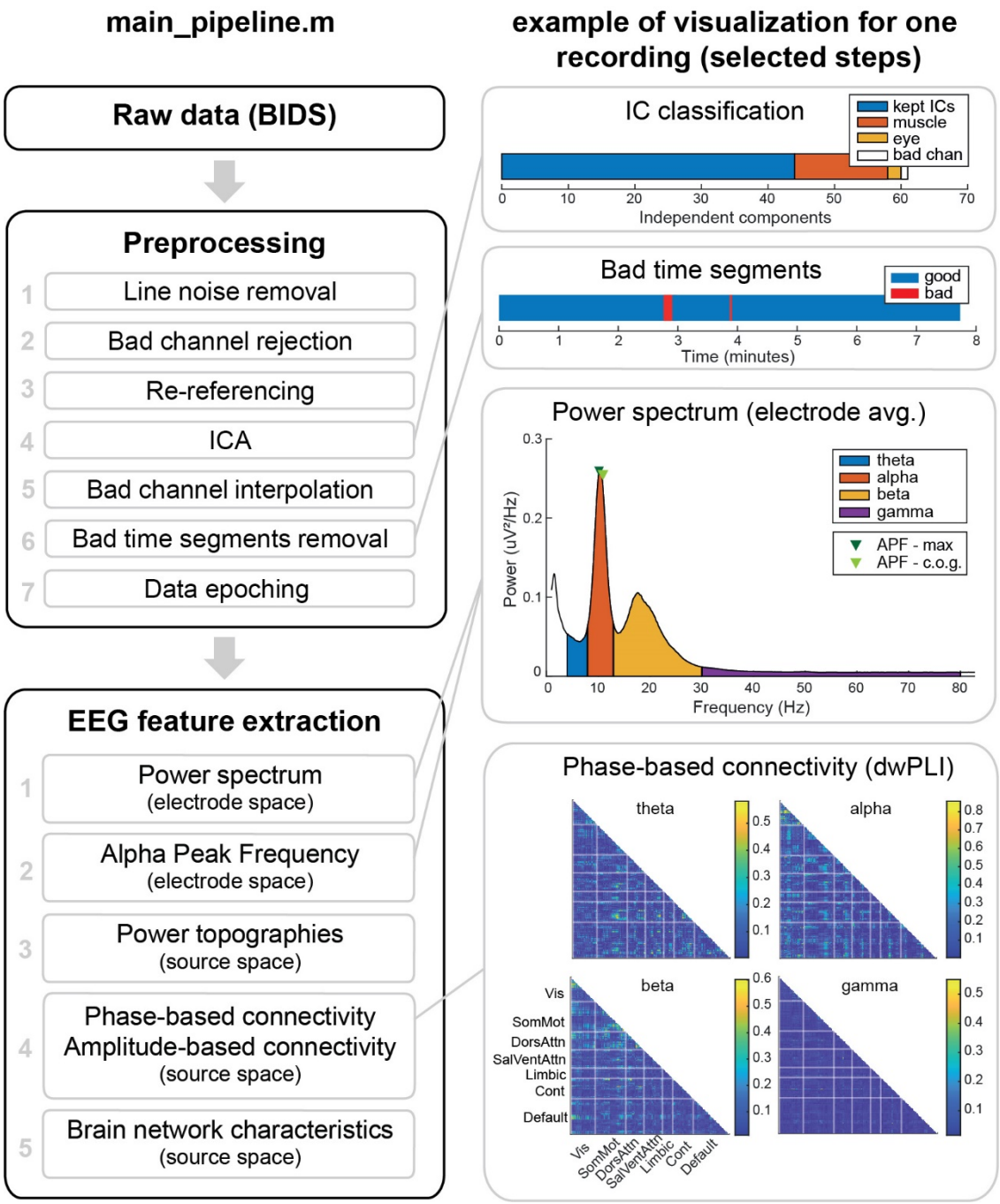

Figure 1. Outline of the DISCOVER pipeline. The left column shows all preprocessing steps and extracted EEG features. The right column shows visualizations for selected steps and features for one EEG recording of the LEMON dataset. APF = Alpha Peak Frequency; BIDS = Brain Image Data Structure; c.o.g. = center of gravity; Cont = Control; DorsAttn = Dorsal Attention; dwPLI = debiased weighted Phase Lag Index; ICA = Independent Component Analysis; SalVentAttn = Salience-Ventral Attention; SomMot = Somato-Motor; Vis = Visual.

Preprocessing

Automatic preprocessing of EEG data favors objectivity, replicability and speed of EEG preprocessing. Thus, in recent years, notable efforts have been made to automatize the preprocessing of EEG data. Contributions to single preprocessing steps, such as the EEGLab

plugin ICLabel for automatic classification of artifactual independent components[12] and early-step preprocessing pipelines such as PREP have been proposed. Moreover, full automatic preprocessing pipelines have been published for specific populations and settings, including pediatric populations[15,27] and mobile brain-body imaging[28], and specifically focusing on Event Related Potentials (ERP) or resting-state study designs[13,14,29,30]. Our pipeline builds upon these advances and extends them by adding an automatic computation and visualization of physiologically meaningful EEG features that can serve as potential biomarkers. We followed a pragmatic approach towards preprocessing and adopted a simple, established and automatic workflow in EEGLab proposed by Pernet et al.[14] and originally developed for ERP data. We adapted the pipeline to resting-state data and detail the seven preprocessing steps below.

Loading the data

The input of the pipeline must be EEG data in BIDS format[19], including all mandatory sidecar files. We recommend to check the BIDS-compliance with the BIDS validator (http://bids-standard.github.io/bids-validator/). By default, only EEG channels with standard electrode positions in the 10-5 system[31] are preprocessed. However, it is possible to preprocess non-standard channels if all electrode positions and their coordinate system are specified in the pertinent BIDS sidecar file. Optionally, after loading, the data can be downsampled to a frequency specified by the user after the application of an anti-aliasing filter.

1. Line noise removal

Line noise is removed with the EEGLab function *pop_cleanline()*. The CleanLine plugin adaptively estimates and removes sinusoidal artifacts using a frequency-domain (multi-taper) regression technique. CleanLine, as compared to band-stop filters, does not introduce gaps in the power spectrum and avoids the frequency distortions created by filters. This step was added to the Pernet et al.[14] pipeline to explore brain activity at gamma frequencies (> 30 Hz). The line noise frequency (e.g., 50 Hz or 60 Hz) must be specified in the BIDS file *sub-<label>_eeg.json* to be appropriately removed.

2. High pass filtering and bad channel rejection

Artifactual channels are detected and removed with the function *pop_clean_rawdata().* The first step of this function is the application of a high pass filter with the function *clean_drifts()* with a default transition band of 0.25 to 0.75 Hz. A channel is considered artifactual if it meets any of the following criteria: 1) If it is flat for more than 5 seconds, 2) If the z-scored noise-to-signal ratio of the channel is higher than a threshold set to 4 by default, 3) If the channel time course cannot be predicted from a randomly selected subset of remaining channels at least 80% of the recorded time. Channels marked as artifactual are removed from the data. The mentioned parameters are the defaults proposed by Pernet et al.[14].

3. Re-referencing

Data is re-referenced to the average reference with the function *pop_reref()*. Optionally, the time course of the original reference channel can be reconstrued and added back to the data if the user specifies it in *define_params*. The name of the reference electrode name must be specified in the BIDS file *sub-<label>_eeg.json*.

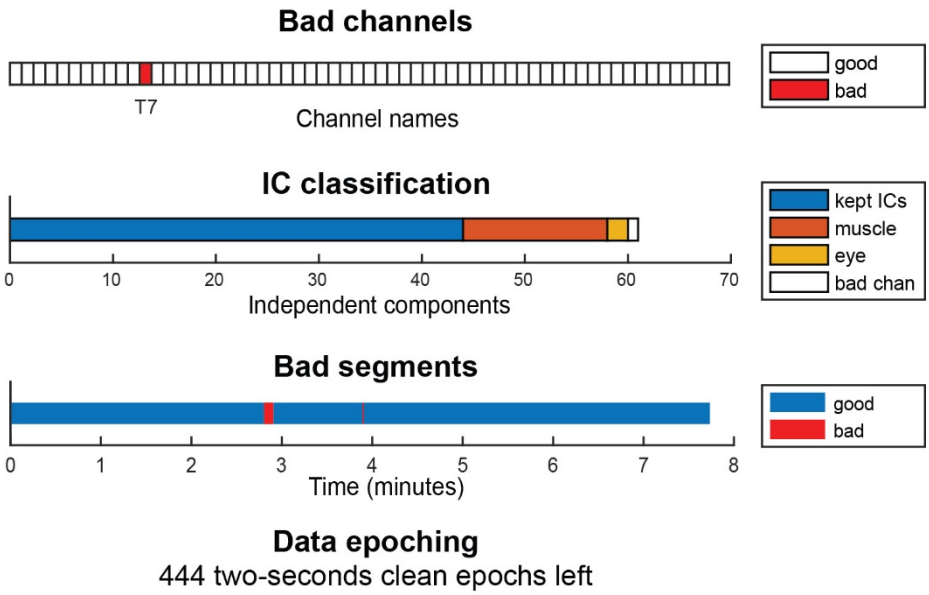

Figure 2. Visualization of the outcome of the preprocessing part of the DISCOVER pipeline. Example of one EEG recording of the LEMON dataset. In the independent component classification (second row), bad channels correspond to the channels that were removed in the bad channel removal step (first row). Bad channels were not included in the independent component analysis. IC = independent component.

4. Independent Component Analysis and automatic IC rejection

Independent Component Analysis (ICA) is performed with the function *pop_runica()* using the algorithm *runica*. Artifactual components are automatically classified into seven distinct categories ('Brain', 'Muscle', 'Eye', 'Heart', 'Line Noise', 'Channel Noise' and 'Other') by the ICLabel classifier[12]. Note that ICA is performed only on clean channels, as bad channels detected in step 2 were removed from the data. Therefore, the category 'Channel Noise' in the IC classification refers to channel noise remaining after bad channel removal in step 2. By default, only components whose probability of being 'Muscle' or 'Eye' is higher than 80% are subtracted from the data[14]. Due to the heuristic non-deterministic nature of the ICA algorithm, its results vary across repetitions. That is, every repetition of the ICA algorithm leads to small differences in the reconstructed time series after the removal of artifactual components. While these deviations are small, we noticed that they affect the removal of bad time segments (step 6). For that reason, the pipeline performs 10 times steps 4, 5 and 6 and selects the bad time segment mask that is most similar to the average bad time segment mask across all repetitions. This reduces the variability of rejected time segments markedly.

5. Interpolation of removed channels

Channels that were removed in step 2 are interpolated with the function *pop_interp()* using spherical splines[32]. This step was added to the Pernet et al.[14] pipeline to hold the number of channels constant across participants.

6. Bad time segment removal

Time segments containing artifacts are removed with the Artifact Subspace Reconstruction (ASR) method[33] implemented in the function *pop_clean_rawdata()*. This method automatically removes segments in which power is abnormally strong. First, a clean segment of data is identified according to the default ASR settings and used for calibration. Calibration data contains all datapoints in which less than 7.5% of channels are noisy. Here, a channel is defined as noisy if the standard deviation of its RMS is higher than 5.5. Therefore, the length of the calibration data depends on the specific recording. Then, in a sliding window fashion, the whole EEG signal is decomposed via PCA and the principal subspaces of the window

segment are compared with those of the calibration data. Segments with principal subspaces deviating from the calibration data (20 times higher variance) are removed. Again, default parameters are in line with Pernet et al.[14].

7. Data segmentation into epochs

Lastly, the continuous data are segmented into epochs with the function *pop_epoch().* By default, data are segmented into 2-second epochs with a 50% overlap. Epochs containing a discontinuity (e.g. because a segment containing an artifact was discarded) are rejected automatically. Data segmentation was adapted from Pernet et al.[14], which focused on event-related data. The proposed epoch length was chosen to establish a balance between the stationarity of the signal and the reliability of the later extracted features.

EEG feature extraction

The multiple possibilities of analyzing EEG data pose a challenge when deciding which brain features to analyze. Here, we focused on a reduced set of features that can be physiologically interpreted, as explainable biomarkers have more chances to be clinically useful[1].

In electrode space features based on the power spectra of the EEG signal. Specifically, power in the theta (4 to < 8 Hz), alpha (8 to < 13 Hz), beta (13 to 30 Hz) and gamma (> 30 to 80 Hz) bands is extracted, with the band limits defined by the COBIDAS-MEEG guidelines[34] and maintained throughout all features. Furthermore, the Alpha Peak Frequency (APF), i.e. the frequency at which a peak in the power spectrum in the alpha range occurs, is determined. Power changes in these frequency bands have been found in a broad spectrum of neuropsychiatric disorders[35]. In addition, there is evidence that the APF correlates with behavioral and cognitive characteristics[36] in aging and disease[37].

In source space, we extract features based on functional connectivity and graph measures that characterize brain networks. Functional connectivity measures constitute promising biomarker candidates in neuropsychiatric disorders[16,17]. In EEG, functional connectivity measures are commonly classified as either phase-based or amplitude-based. These two types of connectivity capture different and complementary communication processes in the brain[38]. This pipeline thus includes two connectivity measures with low susceptibility to volume conduction: the phase-based debiased weighted Phase Lag Index (dwPLI)[39] and the amplitude-based orthogonalized Amplitude Envelope Correlation (AEC)[40]. Both connectivity measures are assessed in source space in the four frequency bands mentioned before (theta, alpha, beta, and gamma). Furthermore, this pipeline characterizes brain networks using common graph theory measures[41]. For each connectivity measure and frequency band, we compute two local graph measures for each source location: the degree and the clustering coefficient. We further compute three global graph measures that characterize the whole network: the global clustering coefficient, the global efficiency and the smallworldness.

Power and connectivity features are computed using the preprocessed and segmented data in FieldTrip. Graph theory measures are computed with the Brain Connectivity Toolbox[41]. Specific parameters on feature extraction are defined in the function *define_params* and detailed below.

1. Power spectrum

Power spectra are computed with the FieldTrip function *ft_freqanalysis* between 1 and 100 Hz using Slepian multitapers with +/-1 Hz frequency smoothing. For 2-second epochs, the maximum frequency resolution of the power spectrum is by definition the inverse of the epoch length, i.e. 0.5 Hz. As frequency band limits are determined by the spectral resolution, the pipeline zero-pads the epochs to 5 seconds, which yields a resolution of 0.2 Hz, to better capture the frequency range of the bands. Thus, the frequency band limits for theta, alpha, beta and gamma are 4 to 7.8 Hz, 8 to 12.8 Hz, 13 to 30 Hz and 30.2 to 80 Hz, respectively.

Power spectra are computed for every channel and then averaged across epochs and channels to obtain a single global power spectrum. This global power spectrum is saved to *sub-<label>_power.mat* files and visualized with the different frequency bands highlighted in different colors (Figure 3).

2. Alpha Peak Frequency

APF is computed based on the global power spectrum in the alpha range (8 to 12.8 Hz). As there are different strategies for computing the APF, the two most often reported in the literature[42] are calculated: the frequency at which the highest peak occurs (peak maximum) and the center of gravity (c.o.g.) of the alpha band. The peak maximum is computed with the Matlab function *findpeaks()*. If there is no peak in the alpha range, no value is returned. The center of gravity is computed as the power-weighted average of frequencies in the alpha band. Both measures are visualized in the same figure depicting the power spectrum averaged across channels and epochs (Figure 3). Individual APF values are also saved to the *sub-<label>_peakfrequency.mat* files.

3. Source reconstruction

To mitigate the volume conduction problem when computing functional connectivity measures[43], we perform a source reconstruction of the preprocessed data with an atlas-based beamforming approach. For each frequency band, the band-pass filtered data from sensor space is projected into source space using an array-gain Linear Constrained Minimum Variance (LCMV) beamformer[44]. As source model, we selected the centroids of 100 regions of interest (ROIs) of the 7-network version of the Schaefer atlas[45]. This atlas is a refined version of the Yeo atlas and follows a data-driven approach in which 100 parcellations are clustered and assigned to 7 brain networks (Visual, Somato-Motor, Dorsal attention, Salience-Ventral attention, Limbic, Control, and Default networks). The lead field is built using a realistically shaped volume conduction model based on the template of the Montreal Neurological Institute (MNI) available in FieldTrip (*standard_bem.mat*) and the source model. Spatial filters are finally constructed with the covariance matrices of the band-passed filtered data and the described lead fields. A 5% regularization parameter is set to account for rank deficiencies in the covariance matrix and the dipole orientation is fixed to the direction of the maximum variance following the most recent recommendations[46]. An estimation of the power for each source location is obtained using the spatial filter and band-passed data. A visualization of the source power in each frequency band (Figure 3) is provided by projecting the band-specific source power to a cortical surface model provided as template in FieldTrip (*surface_white_both.mat*).

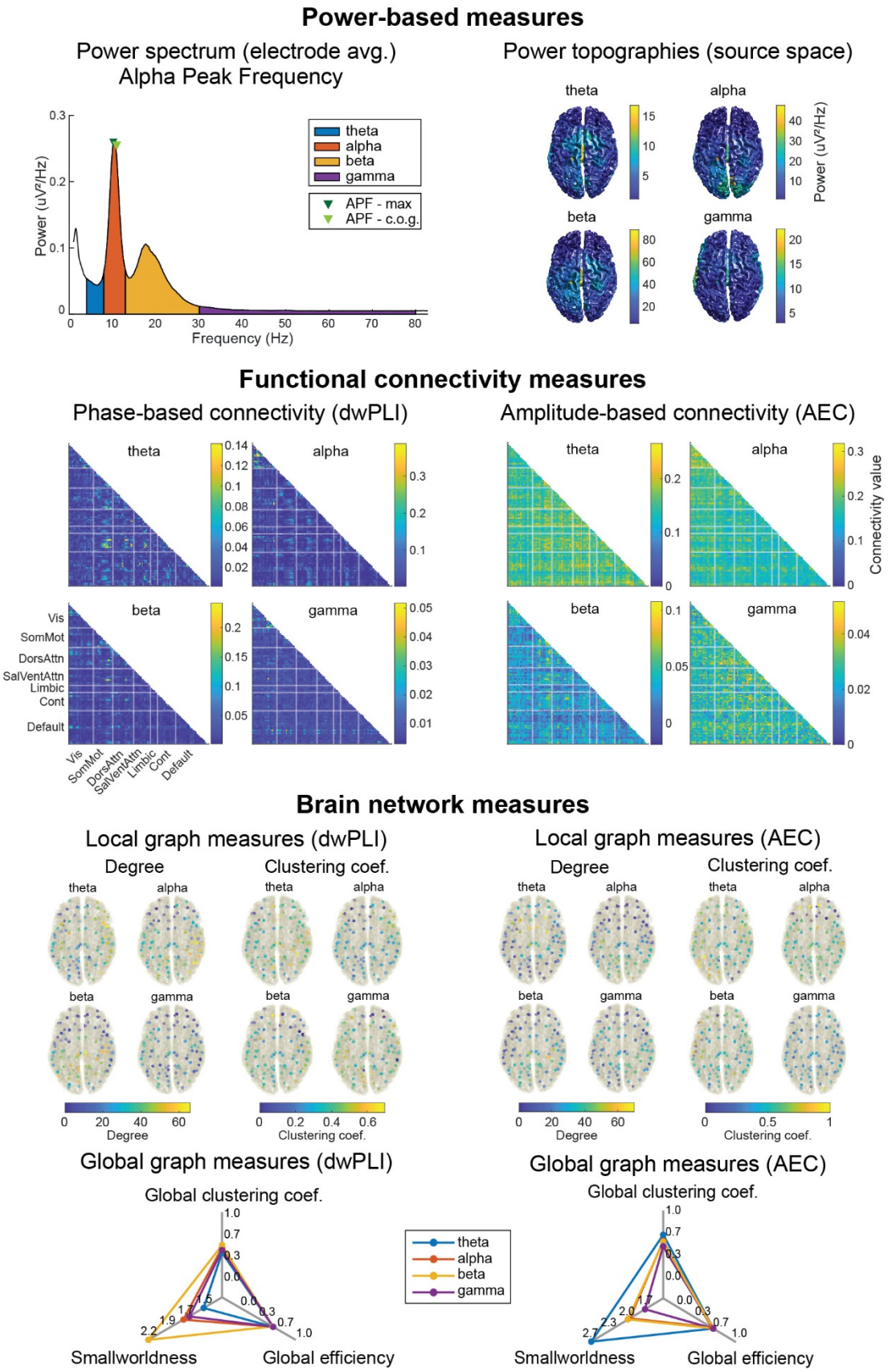

Figure 3. Visualization of the outcome of the feature extraction part of the pipeline. Example for one recording of the LEMON dataset (same recording as Figure 2). **Power-based measures** are extracted in electrode (power spectrum averaged across channels, APF) and source space (power topographies). **Functional connectivity measures** are estimated in source space for 100 pairs of brain regions organized in 7 different functional networks (Visual, Somato-Motor, Salience, Ventral-Attention, Limbic, Control, and Default). **Brain network**

measures are characterized by local (degree and clustering coefficient) and global (global clustering coefficient, global efficiency and smallworldness) graph measures computed on the thresholded connectivity matrices. AEC = Amplitude Envelope Correlation; APF = Alpha Peak Frequency; c.o.g. = center of gravity; Cont = Control; DorsAttn = Dorsal Attention; dwPLI = debiased weighted Phase Lag Index; SalVentAttn = Salience-Ventral Attention; SomMot = Somato-Motor; Vis = Visual.

4. Functional connectivity

After the creation of spatial filters in the four frequency bands, virtual time series in the 100 source locations are reconstructed for each frequency band by applying the respective band-specific spatial filter to the band-pass filtered sensor data. Then, the two functional connectivity measures (dwPLI and AEC) are computed for each frequency band and for each combination of the 100 reconstructed virtual time series. Average connectivity matrices for each band are visualized (Figure 3) and saved to separate files (*sub-<label>_<conmeasure>_<band>.mat*).

The phase-based connectivity measure dwPLI is computed using the FieldTrip function *ft_connectivityanalysis* with the method *wpli_debiased*, which requires a frequency structure as input. Therefore, Fourier decompositions of the virtual time series are calculated in each frequency band with a frequency resolution of 0.5 Hz. Thereby, a connectivity matrix is obtained for each frequency of interest in the current frequency band. Connectivity matrices are then averaged across each frequency band resulting in one 100x100 connectivity matrix for each of the four frequency bands.

The amplitude-based connectivity measure AEC is computed according to the original equations with a custom function *compute_aec*, as the original implementation was not available in FieldTrip. For each epoch, the analytical signal of the virtual time series is extracted at each source location with the Hilbert transform. For each source pair, the analytical signal at source A is orthogonalized with respect to the analytical signal at source B, yielding the signal $A_{\perp B}$. Then, the Pearson correlation is computed between the amplitude envelope of signals B and $A_{\perp B}$. To obtain the average connectivity between sources A and B, the Pearson correlation between the amplitude envelopes of analytical signal A and signal $B_{\perp A}$ is also computed and the two correlations coefficients are averaged. In this way, we obtain a 100x100 connectivity matrix for each epoch. We finally average the connectivity matrices across epochs, resulting in one 100x100 connectivity matrix for each of the four frequency bands.

5. Brain network characteristics

Graph measures were computed on thresholded and binarized connectivity matrices[41]. Matrices were binarized by keeping the 20% strongest connections. This is an arbitrary threshold and it is good practice to test the reliability of results with different binarizing thresholds[47]. This threshold can be easily changed in the function *define_params*.

The computed local measures are the degree and the clustering coefficient. The degree is the number of connections of a node in the network. The clustering coefficient is the percentage of triangle connections surrounding a node. The measures, thus, assess the global and local connectedness of a node, respectively.

The computed global measures are the global clustering coefficient, the global efficiency and the smallworldness. The global clustering coefficient is a measure of functional segregation in the network and is defined as the average clustering coefficient of all nodes. The global efficiency is a measure of functional integration in the network and is defined as the average of the inverse shortest path length between all pairs of nodes. High global efficiency indicates that information can travel efficiently between regions that are far away. Smallworldness compares the ratio between functional integration and segregation in the network against a random network of the same size and degree. Smallworld networks are highly clustered and have short characteristic path length (average shortest path length between all nodes)

compared to random networks[48]. Local and global measures are visualized per recording and saved to files named *sub-<label>_graph_<conmeasure>_<band>.mat* (Figure 3).

RESULTS

Testing the DISCOVER-EEG pipeline in two large, public datasets

We applied the DISCOVER-EEG pipeline to two openly-available resting state EEG datasets: the LEMON dataset[20] including 212 young and old healthy participants and the Chronic pain dataset, unpublished until now, which includes 74 patients with chronic pain recorded with a mobile dry-electrode EEG system (Figure 4). The application of DISCOVER-EEG to the LEMON dataset exemplifies how to reuse a public dataset and inspire the discovery of new biomarkers (please refer to the next Results section). The application to the Chronic pain dataset exemplifies how to speed up biomarker discovery in a clinical population and setting. The application of the pipeline to this second dataset was initially conceived as a proof of concept to test a dry-EEG system in translational research. However, the acquisition of 74 EEG resting recordings within only 7 months, together with the fast and objective processing of the data, evidence the utility of new hardware advances and processing methods for the fast discovery of clinically-relevant brain biomarkers. Below we detail the characteristics of both datasets used, as well as the outcome of their preprocessing with the DISCOVER-EEG pipeline. This latter report could be of use in future studies interested in benchmarking different EEG configurations or EEG preprocessing strategies.

LEMON dataset

The LEMON dataset is a publicly available resting state EEG dataset of 212 young and old healthy participants acquired in Leipzig (Germany) to study mind-body-emotion interactions[20]. This dataset is divided into two groups based on the age of the participants: a 'young' group (20 to 35 years old; N = 141; 43 females) and an 'old' group (55 to 80 years old; N = 70; 35 females). One participant (male) had an intermediate age and was not included in the posterior statistical analyses (next Results section). Resting state EEG was recorded with a BrainAmp MR plus amplifier using 62 active ActiCAP electrodes (61 scalp electrodes in the 10-10 system positions and 1 VEOG below the right eye) provided by Brain Products Gmbh, Gilching, Germany. The ground electrode was located at the sternum and the reference electrode was FCz. Recording sampling rate was 2500 Hz. Recordings contained 16 blocks of 1-minute duration, 8 with eyes closed and 8 with eyes open in an interleaved fashion. Here, we only analyzed resting state with eyes closed. In consequence, before the execution of the pipeline, all blocks corresponding to eyes-closed resting state were extracted and concatenated, including boundaries between blocks. Two recordings were discarded because the data was truncated. Therefore, 210 eyes-closed resting state recordings of 8 minutes duration were entered to the pipeline.

Chronic pain dataset

The Chronic pain dataset is part of an ongoing project on biomarker discovery in patients suffering from chronic pain (ClinicalTrials.gov, NCT05261243) and is openly available at OSF (see section *Data availability*). This study has been approved by the ethics committee of the TUM School of Medicine with the reference number 6/22 S-KH. To date, the dataset includes 74 patients with chronic pain of mixed etiologies (22 to 85 years old, 41 females), who were recorded between March and November 2022. Resting-state recordings with eyes closed were carried out in a clinical setting with a mobile, dry-electrode EEG setup with 29 scalp electrodes (CGX Quick-32r, Cognionics Inc.) located in the 10-20 system. Ground and reference electrodes were located at the left ear (A1). Recording sampling rate was 500 Hz. Recordings have an average duration of 5 minutes.

DISCOVER-EEG preprocessing outcome for both data sets

After applying the DISCOVER-EEG pipeline to the LEMON dataset, 2 ± 2 channels (mean ± std.) were rejected on average, 7 ± 4 independent components were marked as 'muscle' or 'eye' artifacts and subtracted from the data and 32 ± 42 seconds were labeled as bad

segments, leading to an average of 395 ± 58 clean 2-second epochs per recording. Similarly, in the chronic pain dataset, an average of 5 ± 3 channels (mean ± std.) were rejected, 1 ± 1 independent components were marked as 'muscle' or 'eye' artifacts and subtracted from the data and 66 ± 67 seconds were labeled as bad segments, leading to an average of 221 ± 78 clean 2-second epochs per recording. Figure 4 shows an overview of the preprocessing results for both datasets to give the reader an intuition of how the preprocessing part of the pipeline performs in two datasets with very different characteristics. Considering that recordings were performed in healthy vs. patient populations, these results point to a fair amount of data remaining after the preprocessing of dry-EEG recordings. This is in line with the results of a recent study showing that dry-electrode EEG setups present a similar quality to recordings acquired with active wet electrodes[49]. This could be very useful for the fast acquisition of new datasets and, hence, for clinical biomarker discovery.

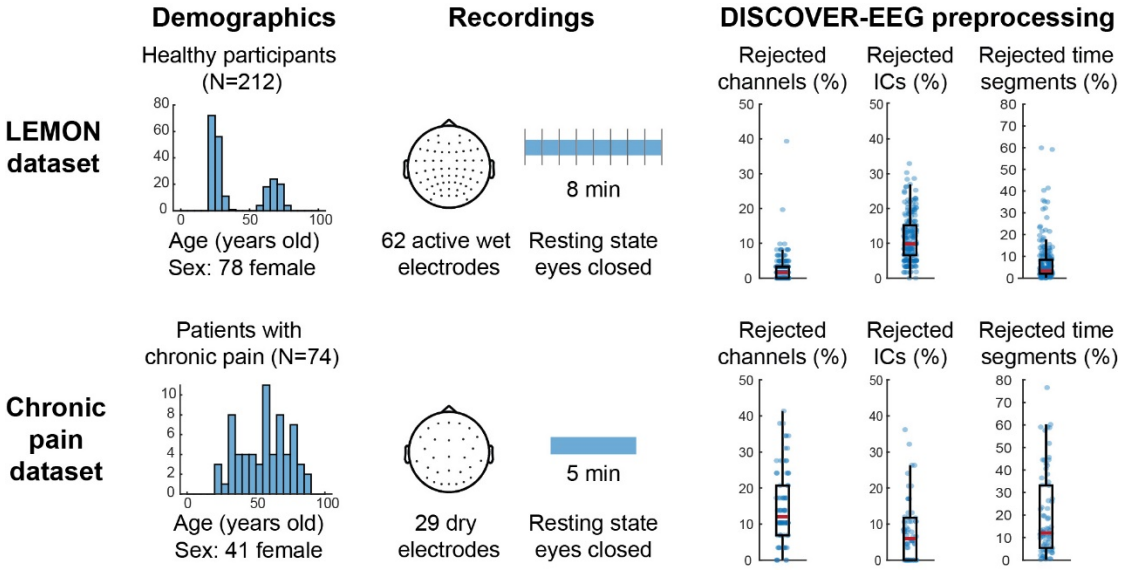

Figure 4. Overview of the datasets used to test the DISCOVER-EEG pipeline and the results of their preprocessing. **Demographics** include histograms depicting the age of the participants in bins of 5 years. **Recordings** depict the layout of the EEG setup and the average duration of the recordings. Vertical bars in the LEMON recordings represent the 1-minute blocks in which the data was acquired. **DISCOVER-EEG preprocessing** presents the preprocessing variables expressed in percentage relative to the number of electrodes (rejected channels, rejected ICs) or length of the recording (rejected time segments). Boxplots visualize the distribution of these variables. The median is indicated by a red horizontal line and the first and third quartiles indicated with the black boxes. The whiskers extend to 1.5 times the interquartile range. Blue dots overlaid to the boxplots represent the individual recordings of each dataset. ICs = Independent Components.

Using DISCOVER-EEG to inspire explainable, age-related biomarkers

Preventive medicine is essential in clinical care. Therefore, non-invasive biomarkers aiming to detect risk factors for certain diseases in the general population are very much sought after. Recently, the measure of brain age, i.e. the expected level of cognitive function of a person with the same chronological age, has been proven a useful marker of cognitive decline in heathy and clinical populations[50,51]. Brain age is usually estimated by machine learning models trained to predict the chronological age of a participant based on neuroimaging data. One criticism of these methods is their limited neuroscientific interpretability, as it is not transparent which features the models use to predict brain age[50]. It would be therefore highly useful to explore which physiologically meaningful brain features change with age, as they could potentially turn into explainable biomarkers predictive of cognitive decline and neurodegeneration. Traditional neuroimaging studies have already shown correlations between healthy ageing and functional and structural changes in the brain[52]. In the EEG field specifically, alterations of brain features, such as a reduction (slowing) of APF and a general

decrease of functional connectivity and network integrity, have been associated with healthy ageing and cognitive decline[53,54].

To demonstrate the use of the DISCOVER-EEG pipeline for predictive biomarker discovery, we explored age-related differences in resting state EEG in the LEMON dataset. These EEG features could eventually turn into predictive or risk biomarkers of neurodegeneration and cognitive decline after extensive validation.

Example analysis: age-related differences in resting state EEG

To demonstrate the value of DISCOVER-EEG for the identification of age-related differences in physiologically explainable EEG features, we conducted an exploratory analysis of the LEMON dataset. To this end, we statistically compared the features automatically extracted by the pipeline in the 'old' and 'young' groups using Bayesian statistics performed in Matlab with the bayesFactor package[55]. As the aggregation of the automatically extracted single-participant features for group analysis can be challenging for the unexperienced user, we have added the script used to perform this group analysis and the visualization of group-level data to the pipeline code (Figure 5).

We tested whether old participants had different APF values than young participants with two-sided independent samples Bayesian t-tests. Two tests were performed, one for each APF measure (the local maximum and the center of gravity). Results show very strong evidence in favor of the alternative hypothesis, i.e. a lower APF in the old compared to the young group, when the APF is computed as local maximum peak (BF_{10} = 325.5), but inconclusive evidence when the APF is computed as the center of gravity (BF_{10} = 1.1) (Figure 5, first row).

We further tested whether there were differences in the connectivity matrices between young and old participants. For each connectivity measure (dwPLI and AEC) and frequency band (theta, alpha, beta, and gamma), we compared the connectivity values of each undirected source pair between the young and the old groups. Thus, we performed 9900 two-sided independent samples Bayesian t-tests per connectivity matrix. In Figure 5, second row, we depict t-values color-coded to show the direction of effects. Statistical tests showing strong evidence in favor ($BF_{10} > 30$) or against ($BF_{10} < 1/30$) the alternative hypothesis are not faded out. We observed strong evidence in favor of a reduction of phase-based connectivity in old participants predominantly in the alpha band as well as a reduction of amplitude-based connectivity (Figure 5, second row, non-masked blue values).

We finally tested whether there were any differences between old and young participants in the graph measures. For the local graph measures, we performed one test per source location, i.e. 100 independent sample Bayesian t-tests for each graph measure, connectivity measure and frequency band. For the global measures, we performed a two-sided independent sample Bayesian t-test per graph measure, connectivity measure and frequency band. With regard to global measures, most prevalent differences appeared at low frequencies (theta and alpha) using the AEC (Figure 5, third row, blue and red dots in brain sketches have $BF_{10} > 30$). The strongest effects with regard to global measures are a reduction of global efficiency and smallworldness of the older group in the beta band for the dwPLI, and the alpha band for the AEC (Figure 5, third row, raincloud plots with inset BF_{10} indicating strong evidence). Together, these results show a reduction of local connectivity at theta and alpha frequencies and an increase of network integration at alpha and beta frequencies in older participants.

Overall, the current findings are in line with previous EEG literature, which has reported a slowing of APF and a general decrease of functional connectivity and network integrity[53,54]. These EEG features confirmed using DISCOVER-EEG are thus promising candidates for predictive or risk biomarkers of healthy ageing. Naturally, their use as clinical biomarkers requires thorough validation beyond the scope of this manuscript.

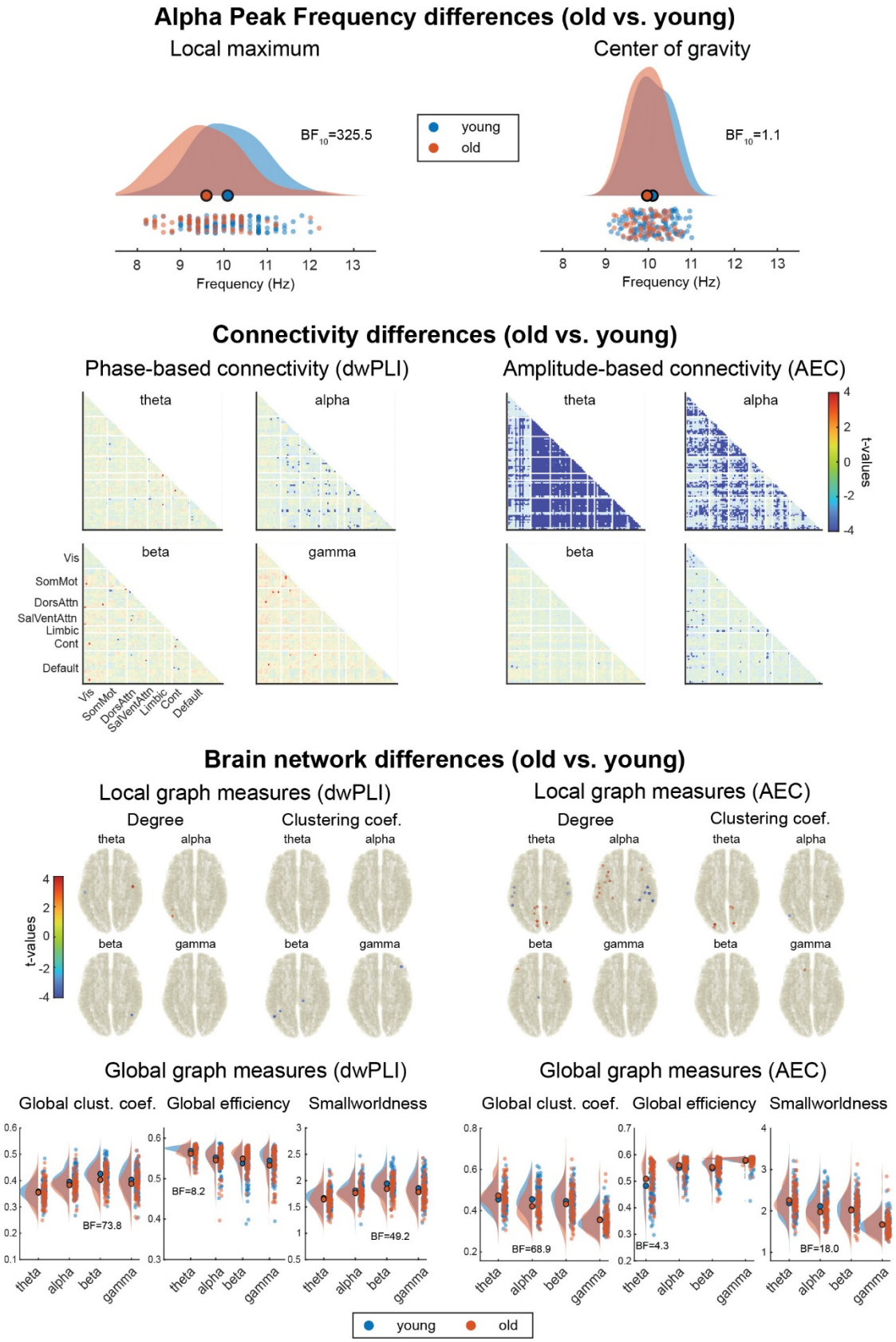

Figure 5. Age-related differences in resting state EEG between old and young participants of the LEMON dataset. **Alpha Peak Frequency differences** between the old and the young group are visualized using raincloud plots[56]. **Connectivity differences** between the old and young group. Blue values indicate lower connectivity in the old group. All connections not showing strong evidence for or against a connectivity difference ($1/30 < BF_{10} < 30$) are faded out. **Brain network differences** between the old and young group. With regard to local graph measures, only locations with strong evidence for ($BF_{10} > 30$) or against ($BF_{10} < 1/30$) a

difference in the graph measures are depicted. Only results in favor of a difference between groups were found (blue dots indicate lower local graph measures in the old group, red dots indicate higher local graph measures in the old group). With regard to global graph measures, only BF_{10} showing substantial evidence for ($BF_{10} > 3$) or against ($BF_{10} < 1/3$) the alternative hypothesis were included as insets to facilitate the reading. AEC = Amplitude Envelope Correlation; BF = Bayes Factor; Cont = Control; DorsAttn = Dorsal Attention; dwPLI = debiased weighted Phase Lag Index; SalVentAttn = Salience-Ventral Attention; SomMot = Somato-Motor; Vis = Visual

DISCUSSION

Here, we present DISCOVER-EEG, an open and fully automated pipeline that enables fast and easy aggregation, preprocessing, analysis and visualization of resting state EEG data. The current pipeline builds upon state-of-the-art automated preprocessing elements and extends them by including the computation and visualization of physiologically relevant EEG features. These EEG features are based on recent COBIDAS guidelines for MEEG research, are implemented in widely-used EEG toolboxes and have been repeatedly associated with cognitive and behavioral measures in healthy as well in neuropsychiatric populations. Therefore, they could represent promising biomarker candidates, which can now easily be extracted using the pipeline.

Importantly, this pipeline presents one out of many ways of preprocessing and analyzing resting state data and is not intended to be the ultimate solution for EEG analysis. Instead, it aims to represent a reasonable and pragmatic realization for accelerating the acquisition, preprocessing and analysis of large-scale datasets with the potential to discover clinically useful biomarkers. For that reason, we adopted a previously published, simple and robust preprocessing strategy and selected a reduced and well-defined set of EEG features that could be useful for biomarker discovery. It is therefore foreseeable that this pipeline might not suit certain populations, settings or research paradigms, such as children, real-life ecological EEG assessments or paradigms assessing event related potentials. However, it is compatible with different types of EEG set-ups, including mobile headsets with dry-electrodes, and its focus on resting state data makes it suitable for patient and healthy populations. The adaptation, extension or modification to the specific needs of the user it is relatively simple due to the modular configuration of the code. By substituting, removing or adding a specific function of the preprocessing or feature extraction the corresponding step would be modified, omitted or included, respectively.

By default, the pipeline uses a realistically shaped volume conduction model based on the template of the Montreal Neurological Institute (MNI) for source localization. For an optimal accuracy of source reconstruction, individual MRIs or at least individual electrode positions could be recorded along the EEG data. However, this would substantially increase the effort and time needed to acquire data and would hinder the fast generation of large new datasets. For that reason, the pipeline uses a generic template for source localization. However, it might be desirable to have different templates that better reflect the variability of head shapes in the future.

On a broader scope, it should always be considered whether datasets used for biomarker discovery are representative of the complete population of interest or whether they are biased towards young, Caucasian, highly educated populations, as it is often the case[57]. The participants of the studies used here to test the pipeline were recruited based on convenience sampling and, therefore, might not cover the entire population. We firmly believe that the creation and adoption of data standards such as BIDS will help to mitigate this fact by promoting collaboration and data sharing around the world.

Our intention with this pipeline was to push the field of EEG biomarker discovery forward to the acquisition and analysis of large datasets, as needed in neuroimaging and artificial intelligence. Moreover, we believe that the example analyses that we provide serve as a starting point for less specialized researches who want to use complex measures of brain function. Thus, the proposed visualizations are intended as a simple and intuitively accessible representation of these complex brain features.

In conclusion, we hope that our fully automated DISCOVER-EEG pipeline can advance the discovery of EEG-based biomarkers in neuropsychiatric disorders. Beyond, we hope that DISCOVER-EEG will promote and facilitate open and reproducible assessments of brain function in EEG communities and beyond.

DATA AVAILABILITY

The LEMON dataset used to exemplify the use of the pipeline is published at doi:10.18112/openneuro.ds000221.v1.0.0 and described in the publication[20]. The dataset used to demonstrate the application of the pipeline to data recorded with a mobile and dry-electrode EEG system is available at https://osf.io/m45j2/ with DOI 10.17605/OSF.IO/M45J2.

CODE AVAILABILITY

The EEG pipeline code is available at https://github.com/crisglav/discover-eeg under the CC-BY-NC-SA 4.0 license.

The pipeline was created and tested in Matlab 2020b (The Mathworks, Inc.) on Ubuntu 18.04.5 LTS with the Signal Processing and Statistical and Machine Learning Toolboxes installed. EEGLab (v2022.0)[58] with the plugins bids-matlab-tools (v6.1), bva-io (v1.7), firfilt, (v2.4), cleanLine (v2.0), ICLabel (v1.3), clean_rawdata (v2.6) and dipfilt (v4.3) were installed and used for preprocessing. FieldTrip (revision ee916f5e5)[22] was used for source reconstruction and EEG feature extraction and the Brain Connectivity Toolbox (version 03 2019)[41] was used for network analysis.

ACKNOWLEDGMENTS

The study has been supported by the TUM Innovation Network Neurotechnology for Mental Health (NEUROTECH), the Deutsche Forschungsgemeinschaft (PL321/14-1) and the TUM School of Medicine (KKF).

AUTHOR CONTRIBUTIONS

- Conceptualization: C.G.A. and M.P.
- Methodology: C.G.A. and M.P.
- Software: C.G.A., F.S.B., J.G.
- Validation: C.G.A., F.S.B., J.G.
- Formal analysis: C.G.A.
- Investigation: C.G.A. and P.T.Z.
- Data curation: C.G.A.
- Visualization: C.G.A. and M.P.
- Writing – Original draft: C.G.A. and M.P.
- Writing – Review and editing: C.G.A., F.S.B., L.T., V.D.H., E.S.M., M.M.N., P.T.Z., J.G. and M.P.
- Supervision: M.P.
- Project administration: M.P.
- Funding acquisition: M.P

COMPETING INTERESTS

The authors declare no competing interests.

REFERENCES

1 Woo, C. W., Chang, L. J., Lindquist, M. A. & Wager, T. D. Building better biomarkers: brain models in translational neuroimaging. *Nat Neurosci* **20**, 365-377, doi:10.1038/nn.4478 (2017).

2 Group, F.-N. B. W. (2016).

3 Botvinik-Nezer, R. *et al.* Variability in the analysis of a single neuroimaging dataset by many teams. *Nature* **582**, 84-88, doi:10.1038/s41586-020-2314-9 (2020).

4 Marek, S. *et al.* Reproducible brain-wide association studies require thousands of individuals. *Nature* **603**, 654-660, doi:10.1038/s41586-022-04492-9 (2022).

5 Drysdale, A. T. *et al.* Resting-state connectivity biomarkers define neurophysiological subtypes of depression. *Nature medicine* **23**, 28-38, doi:10.1038/nm.4246 (2017).

6 Wu, W. *et al.* An electroencephalographic signature predicts antidepressant response in major depression. *Nat Biotechnol*, doi:10.1038/s41587-019-0397-3 (2020).

7 Zhang, Y. *et al.* Identification of psychiatric disorder subtypes from functional connectivity patterns in resting-state electroencephalography. *Nat Biomed Eng*, 309-323, doi:10.1038/s41551-020-00614-8 (2021).

8 Toll, R. T. *et al.* An Electroencephalography Connectomic Profile of Posttraumatic Stress Disorder. *Am J Psychiatry*, appiajp201918080911, doi:10.1176/appi.ajp.2019.18080911 (2020).

9 Ta Dinh, S. *et al.* Brain dysfunction in chronic pain patients assessed by resting-state electroencephalography. *Pain*, doi:10.1097/j.pain.0000000000001666 (2019).

10 Pavlov, Y. G. *et al.* #EEGManyLabs: Investigating the replicability of influential EEG experiments. *Cortex*, doi:10.1016/j.cortex.2021.03.013 (2021).

11 Kam, J. W. Y. *et al.* Systematic comparison between a wireless EEG system with dry electrodes and a wired EEG system with wet electrodes. *NeuroImage* **184**, 119-129, doi:10.1016/j.neuroimage.2018.09.012 (2019).

12 Pion-Tonachini, L., Kreutz-Delgado, K. & Makeig, S. ICLabel: An automated electroencephalographic independent component classifier, dataset, and website. *NeuroImage* **198**, 181-197, doi:10.1016/j.neuroimage.2019.05.026 (2019).

13 Pedroni, A., Bahreini, A. & Langer, N. Automagic: Standardized preprocessing of big EEG data. *NeuroImage* **200**, 460-473, doi:10.1016/j.neuroimage.2019.06.046 (2019).

14 Pernet, C. R., Martinez-Cancino, R., Truong, D., Makeig, S. & Delorme, A. From BIDS-Formatted EEG Data to Sensor-Space Group Results: A Fully Reproducible Workflow With EEGLAB and LIMO EEG. *Front Neurosci* **14**, 610388, doi:10.3389/fnins.2020.610388 (2020).

15 Gabard-Durnam, L. J., Mendez Leal, A. S., Wilkinson, C. L. & Levin, A. R. The Harvard Automated Processing Pipeline for Electroencephalography (HAPPE): Standardized Processing Software for Developmental and High-Artifact Data. *Front Neurosci* **12**, 97, doi:10.3389/fnins.2018.00097 (2018).

16 Ploner, M. & Tiemann, L. Exploring Dynamic Connectivity Biomarkers of Neuropsychiatric Disorders. *Trends in cognitive sciences* **25**, 336-338, doi:10.1016/j.tics.2021.03.005 (2021).

17 Bassett, D. S., Xia, C. H. & Satterthwaite, T. D. Understanding the Emergence of Neuropsychiatric Disorders With Network Neuroscience. *Biol Psychiatry Cogn Neurosci Neuroimaging* **3**, 742-753, doi:10.1016/j.bpsc.2018.03.015 (2018).

18 de Lange, S. C. *et al.* Shared vulnerability for connectome alterations across psychiatric and neurological brain disorders. *Nat Hum Behav* **3**, 988-998, doi:10.1038/s41562-019-0659-6 (2019).

19 Pernet, C. R. *et al.* EEG-BIDS, an extension to the brain imaging data structure for electroencephalography. *Sci Data* **6**, 103, doi:10.1038/s41597-019-0104-8 (2019).

20 Babayan, A. *et al.* A mind-brain-body dataset of MRI, EEG, cognition, emotion, and peripheral physiology in young and old adults. *Sci Data* **6**, 180308, doi:10.1038/sdata.2018.308 (2019).

21 Barker, M. *et al.* Introducing the FAIR Principles for research software. *Sci Data* **9**, 622, doi:10.1038/s41597-022-01710-x (2022).

22 Oostenveld, R., Fries, P., Maris, E. & Schoffelen, J. M. FieldTrip: Open source software for advanced analysis of MEG, EEG, and invasive electrophysiological data. *Computational intelligence and neuroscience* **2011**, 156869, doi:10.1155/2011/156869 (2011).
23 Wilkinson, M. D. *et al.* The FAIR Guiding Principles for scientific data management and stewardship (vol 15, 160018, 2016). *Scientific Data* **6**, doi:10.1038/s41597-019-0009-6 (2019).
24 Cella, D. *et al.* The Patient-Reported Outcomes Measurement Information System (PROMIS): Progress of an NIH Roadmap Cooperative Group During its First Two Years. *Medical Care* **45**, S3, doi:10.1097/01.mlr.0000258615.42478.55 (2007).
25 Niso, G. *et al.* Open and reproducible neuroimaging: From study inception to publication. *NeuroImage* **263**, doi:10.1016/j.neuroimage.2022.119623 (2022).
26 Van Rossum, G. a. D., Fred L. *Python 3 Reference Manual*. (CreateSpace, 2009*).
27 Debnath, R. *et al.* The Maryland analysis of developmental EEG (MADE) pipeline. *Psychophysiology* **57**, e13580, doi:10.1111/psyp.13580 (2020).
28 Klug, M. *et al.* The BeMoBIL Pipeline for automated analyses of multimodal mobile brain and body imaging data. *bioRxiv*, 2022.2009.2029.510051, doi:10.1101/2022.09.29.510051 (2022).
29 Bailey, N. *et al.* Introducing RELAX (the Reduction of Electroencephalographic Artifacts): A fully automated pre-processing pipeline for cleaning EEG data - Part 1: Algorithm and Application to Oscillations. *bioRxiv*, 2022.2003.2008.483548, doi:10.1101/2022.03.08.483548 (2022).
30 Rodrigues, J., Weiss, M., Hewig, J. & Allen, J. J. B. EPOS: EEG Processing Open-Source Scripts. *Frontiers in Neuroscience* **15**, doi:10.3389/fnins.2021.660449 (2021).
31 Oostenveld, R. & Praamstra, P. The five percent electrode system for high-resolution EEG and ERP measurements. *Clinical neurophysiology : official journal of the International Federation of Clinical Neurophysiology* **112**, 713-719, doi:10.1016/s1388-2457(00)00527-7 (2001).
32 Perrin, F., Pernier, J., Bertrand, O. & Echallier, J. F. Spherical splines for scalp potential and current density mapping. *Electroencephalogr Clin Neurophysiol* **72**, 184-187 (1989).
33 Mullen, T. R. *et al.* Real-Time Neuroimaging and Cognitive Monitoring Using Wearable Dry EEG. *Ieee Transactions on Biomedical Engineering* **62**, 2553-2567, doi:10.1109/Tbme.2015.2481482 (2015).
34 Pernet, C. *et al.* Issues and recommendations from the OHBM COBIDAS MEEG committee for reproducible EEG and MEG research. *Nat Neurosci* **23**, 1473-1483, doi:10.1038/s41593-020-00709-0 (2020).
35 Newson, J. J. & Thiagarajan, T. C. EEG Frequency Bands in Psychiatric Disorders: A Review of Resting State Studies. *Frontiers in human neuroscience* **12**, 521, doi:10.3389/fnhum.2018.00521 (2018).
36 Haegens, S., Cousijn, H., Wallis, G., Harrison, P. J. & Nobre, A. C. Inter- and intra-individual variability in alpha peak frequency. *NeuroImage* **92**, 46-55, doi:10.1016/j.neuroimage.2014.01.049 (2014).
37 Klimesch, W. EEG alpha and theta oscillations reflect cognitive and memory performance: a review and analysis. *Brain Res Brain Res Rev* **29**, 169-195 (1999).
38 Engel, A. K., Gerloff, C., Hilgetag, C. C. & Nolte, G. Intrinsic coupling modes: multiscale interactions in ongoing brain activity. *Neuron* **80**, 867-886, doi:10.1016/j.neuron.2013.09.038 (2013).
39 Vinck, M., Oostenveld, R., van Wingerden, M., Battaglia, F. & Pennartz, C. M. An improved index of phase-synchronization for electrophysiological data in the presence of volume-conduction, noise and sample-size bias. *NeuroImage* **55**, 1548-1565, doi:10.1016/j.neuroimage.2011.01.055 (2011).
40 Hipp, J. F., Hawellek, D. J., Corbetta, M., Siegel, M. & Engel, A. K. Large-scale cortical correlation structure of spontaneous oscillatory activity. *Nat Neurosci* **15**, 884-890, doi:10.1038/nn.3101 (2012).
41 Rubinov, M. & Sporns, O. Complex network measures of brain connectivity: uses and interpretations. *NeuroImage* **52**, 1059-1069, doi:10.1016/j.neuroimage.2009.10.003 (2010).

42 Corcoran, A. W., Alday, P. M., Schlesewsky, M. & Bornkessel-Schlesewsky, I. Toward a reliable, automated method of individual alpha frequency (IAF) quantification. *Psychophysiology* **55**, e13064, doi:10.1111/psyp.13064 (2018).
43 Bastos, A. M. & Schoffelen, J. M. A Tutorial Review of Functional Connectivity Analysis Methods and Their Interpretational Pitfalls. *Frontiers in systems neuroscience* **9**, 175, doi:10.3389/fnsys.2015.00175 (2015).
44 Van Veen, B. D., van Drongelen, W., Yuchtman, M. & Suzuki, A. Localization of brain electrical activity via linearly constrained minimum variance spatial filtering. *IEEE transactions on bio-medical engineering* **44**, 867-880. (1997).
45 Schaefer, A. *et al.* Local-Global Parcellation of the Human Cerebral Cortex from Intrinsic Functional Connectivity MRI. *Cereb Cortex* **28**, 3095-3114, doi:10.1093/cercor/bhx179 (2018).
46 Westner, B. U. *et al.* A unified view on beamformers for M/EEG source reconstruction. *NeuroImage* **246**, doi:10.1016/j.neuroimage.2021.118789 (2022).
47 Adamovich, T., Zakharov, I., Tabueva, A. & Malykh, S. The thresholding problem and variability in the EEG graph network parameters. *Scientific Reports* **12**, doi:10.1038/s41598-022-22079-2 (2022).
48 Watts, D. J. & Strogatz, S. H. Collective dynamics of 'small-world' networks. *Nature* **393**, 440-442, doi:10.1038/30918 (1998).
49 Marini, F., Lee, C., Wagner, J., Makeig, S. & Gola, M. A comparative evaluation of signal quality between a research-grade and a wireless dry-electrode mobile EEG system. *Journal of neural engineering* **16**, doi:10.1088/1741-2552/ab21f2 (2019).
50 Cole, J. H. & Franke, K. Predicting Age Using Neuroimaging: Innovative Brain Ageing Biomarkers. *Trends Neurosci* **40**, 681-690, doi:10.1016/j.tins.2017.10.001 (2017).
51 Engemann, D. A. *et al.* A reusable benchmark of brain-age prediction from M/EEG resting-state signals. *NeuroImage* **262**, 119521, doi:10.1016/j.neuroimage.2022.119521 (2022).
52 Damoiseaux, J. S. Effects of aging on functional and structural brain connectivity. *NeuroImage* **160**, 32-40, doi:10.1016/j.neuroimage.2017.01.077 (2017).
53 Scally, B., Burke, M. R., Bunce, D. & Delvenne, J. F. Resting-state EEG power and connectivity are associated with alpha peak frequency slowing in healthy aging. *Neurobiol Aging* **71**, 149-155, doi:10.1016/j.neurobiolaging.2018.07.004 (2018).
54 Onoda, K., Ishihara, M. & Yamaguchi, S. Decreased Functional Connectivity by Aging Is Associated with Cognitive Decline. *J Cognitive Neurosci* **24**, 2186-2198, doi:DOI 10.1162/jocn_a_00269 (2012).
55 bayesFactor (10.5281/zenodo.2842910, 2022).
56 Allen, M., Poggiali, D., Whitaker, K., Marshall, T. R. & Kievit, R. A. Raincloud plots: a multi-platform tool for robust data visualization. *Wellcome Open Res* **4**, 63, doi:10.12688/wellcomeopenres.15191.1 (2019).
57 Henrich, J., Heine, S. J. & Norenzayan, A. The weirdest people in the world? *Behav Brain Sci* **33**, 61-83; discussion 83-135, doi:10.1017/S0140525X0999152X (2010).
58 Delorme, A. & Makeig, S. EEGLAB: an open source toolbox for analysis of single-trial EEG dynamics including independent component analysis. *Journal of neuroscience methods* **134**, 9-21 (2004).